nanomaterials

MDPI

Article

Sonochemical-Assisted Biogenic Synthesis of Theophrasite β-Ni(OH)$_2$ Nanocluster Using Chia Seeds Extract: Characterization and Anticancer Activity

Hanaa A. Hassanin [1,2] and Amel Taha [1,3,*]

[1] Department of Chemistry, College of Science, King Faisal University, P.O. Box 400, Al-Ahsa 31982, Saudi Arabia; haessa@kfu.edu.sa
[2] Department of Chemistry, Faculty of Science, Ain Shams University, Abbassia, Cairo 11566, Egypt
[3] Department of Chemistry, Faculty of Science and Technology, Al-Neelain University, Khartoum 11121, Sudan
* Correspondence: ataha@kfu.edu.sa; Tel.: +966-135897506; Fax: +966-135899557

Abstract: Theophrasite β-Ni(OH)$_2$ nanocluster were fabricated via the sonochemical-assisted biogenic method using chia seeds extract as a reducing and stabilizing agent. The optical and morphological feature of the synthesized nanocluster was characterized using UV-Vis, FTIR, FE-SEM-EDS, HR-TEM, DLS, XPS, and XRD analysis. According to FE-SEM and HR-TEM images of the synthesized materials, β-Ni(OH)$_2$ nanocluster illustrates the hexagonal particle shape with an average size of 5.8 nm, while the EDS results confirm the high purity of the synthesized nanocluster. Moreover, the XRD pattern of the synthesized materials shows typical peaks that match the reference pattern of the Theophrasite form of β-Ni(OH)$_2$ with a hexagonal crystal system. The XPS analysis illustrates that the prepared samples exhibit both Ni^{2+} and Ni^{3+} with the predominance of Ni^{2+} species. Additionally the in-vitro cytotoxic activity of β-Ni(OH)$_2$ nanocluster is tested against the MCF7 cell lines (breast cancer cells). The MTT assay results proved that the synthesized β-Ni(OH)$_2$ nanocluster has potent cytotoxic activity against breast cancer cell lines (IC_{50}: 62.7 μg/mL).

Keywords: β-Ni(OH)$_2$; chia extract; nanocluster; cytotoxicity; sonochemical

Citation: Hassanin, H.A.; Taha, A. Sonochemical-Assisted Biogenic Synthesis of Theophrasite β-Ni(OH)$_2$ Nanocluster Using Chia Seeds Extract: Characterization and Anticancer Activity. *Nanomaterials* **2022**, *12*, 1919. https://doi.org/10.3390/nano12111919

Academic Editor: Saura Sahu

Received: 13 April 2022
Accepted: 6 May 2022
Published: 3 June 2022

1. Introduction

Nanoscale materials have recently gained great attention in the scientific disciplines due to their unfamiliar physical and chemical properties compared to their bulk components [1,2]. Many potential applications were reported for these materials such as pharmaceutical research, catalysis, fabrication of semiconductors, electronic manufacturing, and recently medical application, especially for antitumor therapy [3–7]. Various nanoparticles are tested for the in-vitro cytotoxicity on a wide range of cancer cell types [8]. The Toxicity effect depends on the physicochemical properties of metal nanoparticles such as structure and crystal morphology [9]. Huang et al. reported that amorphous TiO_2 nanoparticles have higher reactivity in the generation of reactive oxygen species (ROS) compared to the anatase and rutile analogs. The cubic and octahedron CeO_2 showed a less toxic response toward RAW264.7 cells than the rod-shaped CeO_2 [10]. The charge of the nanomaterial surface may also affect the toxicity influence. The positively charged ZnO nanoparticles showed a higher toxic effect against A549 cells than the negatively charged particles [11]. Different positive charges of Fe nanoparticles (Fe_3O_4, carbon-coated Fe, and oleic acid-coated Fe_3O_4) produced toxic responses in BEL-7402 cells, the worse toxic response was correlated to a higher positive charge [12,13].

For decades, nickel hydroxide was studied and has attracted considerable attention due to its important applications such as photocatalysis [1], oxidation of alcohol as active electrode material, hybrid-super capacitors, and batteries [14]. Furthermore, Ni(OH)$_2$ has been reported to induce inflammation in the lungs of rodents [15].The cytotoxicity of

($Ni(OH)_2$ nanoparticles was examined in a comparison with (NiO) nanoparticles in the range of 10 to 100 μg/mL toward human bronchoalveolar carcinoma (A549) and human hepatocellular carcinoma (HepG2) cell lines. The results demonstrate that $Ni(OH)_2$ was more toxic than NiO nanoparticles [9]. Nickel hydroxide exists in two main crystalline phases (α-$Ni(OH)_2$ and β-$Ni(OH)_2$). α-$Ni(OH)_2$ is stacked randomly along the axis (001) due to the presence of the anions between layers accompanied by water molecules, whereas the β-$Ni(OH)_2$ is perfectly stacked as hexagonal crystals. The morphological control for both morphologies of $Ni(OH)_2$ can be achieved by synthetic conditions as well as the incorporation of polymers or surfactants [16].

Various techniques have been developed for the production of metal nanoparticles with high energy consumption and longer reaction time strategies such as chemical deposition [17], sol-gel technique [18], co-precipitation [19], green methods [20,21], hydrothermal [22], solvothermal and sonochemical synthesis [23]. The sonochemical-assisted synthesis method has several advantages, such as morphology control, homogeneity of mixing, and decreased product agglomeration [24]. Using the green protocol such as plant extracts, Microorganisms, and enzymes in nanoparticle synthesis is a new approach nowadays. The plant extract shows various benefits including the lack of any toxins and contaminants as well as being environmentally safe [25–27]. Recently it has been reported that herbal and medicinal plants were rich in many biologically active components such as flavonoids, amino acids, alkaloids, tannins, terpenoids, saponins, and phenolics which can be responsible for the reduction of metal to metal nanoparticles [27–30].

Salvia hispanica L. is one of the seasonal herbaceous plants that belongs to the Lamiaceae family, commonly known as Chia, it can be found as dark and white small seeds. The chia seeds are well known and valued as high sources of protein, dietary fiber, minerals, polyphenolic compounds, and oils. In addition, Chia is known for high contents of natural antioxidants such as flavonoids, phenolic compounds, caffeic acid, kaempferol, and chlorogenic acid that can be beneficial to human health [31]. These antioxidants can scavenge free radicals, chelate ions, and donate hydrogens [32]. It usually decreases chronic disease risk (cancer and heart attack), and also offers protection against some diseases such as diabetes and Alzheimer's [29]. Chia seeds extract is also known to have antimicrobial efficiency as reported by G. K. Divyapriya et al. [33]. Accordingly, these chemical compounds in the chia seeds extract can be considered a model candidate for the reduction and stabilization process of nanomaterials. The dark or white chia seed extract has been applied in the synthesis of Ag nanoparticles [34], CuO and NiO nanoparticles [35]. In the present work chia seeds extract is employed to synthesize β-$Ni(OH)_2$ nanocluster using the sonochemical assisted biogenic method as a unique, fast, effective, and eco-friendly method. In addition, the in-vitro cytotoxic activity of β-$Ni(OH)_2$ nanocluster is examined against the MCF7 cell lines (breast cancer cells).

2. Excremental and Methods

2.1. Materials

Nickel (II) chloride hexahydrate ($NiCl_2 \cdot 6H_2O$, 99.9%), and potassium hydroxide (KOH, ≥85.0%) were purchased from Sigma-Aldrich, St. Louis, MO, USA. White chia seeds were collected from the local market in Hufof, eastern province, Saudi Arabia.

2.2. Preparation of Chia Extract

4.0 g of chia seeds were crushed, added to deionized water (100 mL), and heated for 15 min at 80 °C then it was double-filtered using a home sieve system and a Whatman filter paper. Finally, the extract was refrigerated at 4 °C for future use.

2.3. Synthesis of β-$Ni(OH)_2$ Nanocluster

For the synthesis of $Ni(OH)_2$ 0.1 M $NiCl_2 \cdot 6H_2O$ was mixed with chia seeds extract with a volumetric ratio (1:1) at room temperature with constant stirring, then the pH was adjusted to 11.0 by dropwise addition of 1.0 M of KOH solution. The pH measurements

were carried out using Orion 2 Star (Thermo Fisher Scientific, Waltham, MA, USA) pH meter. The reaction mixture was then subjected to ultrasonication for 30 min using Power-Sonic 405 (Hwashin, Seoul, Korea) with a working frequency of 40 kHz and a maximum input power of up to 350 W. Finally, the synthesized material was rinsed five times with deionized water and allowed to dry at room temperature.

2.4. Characterization of β-Ni(OH)$_2$ Nanoparticles

Various analytical techniques are used to investigate the chemical and physical properties of the synthesized β-Ni(OH)$_2$. The optical characteristics of the synthesized sample are investigated to confirm the bio-genic synthesis of β-Ni(OH)$_2$ by monitoring the absorption spectra of the solution using a Shimadzu UV–vis spectrophotometer (Kyoto, Japan). DLS (Dynamic light scattering) measurements provide further information about the average hydrodynamic particle diameter (d, nm). FT-IR spectroscopy is used to detect different phytochemical functional groups responsible for the production and stabilization of β-Ni(OH)$_2$. The FT-IR analysis was recorded using a Cary 630 FT-IR spectrophotometer (South San Francisco, CA, USA). To study the surface morphology of the synthesized β-Ni(OH)$_2$, the FE-SEM (Field emission-Scanning electron microscopy) is recorded using FEI, QUANTA FEG, 250 high-resolution field emission electron microscope (Thermo Fisher Scientific, Hillsboro, OR, USA), linked with a high-angle dark-field detector and X-ray energy dispersive spectroscopy device (EDS). Furthermore, TEM images were collected using (JEOL-JEM-2100, JEOL, Peabody, MA, USA) transmission electron microscopy at 90 kV acceleration voltage by dispersing the sample in ethanol by sonication for 30 min and placing one drop of the suspension on the carbon-coated copper grid (400 mesh) and allowed to dry at room temperature. The particle size distribution was calculated using ImageJ software. X-ray diffraction spectroscopy (XRD) was carried out using an Empyrean X-ray diffractometer, Malvern, UK (Cu Ka radiation with a wavelength of 1.54° A) to determine the crystalline phase of the synthesized Ni(OH)$_2$. The nano-crystallite size was calculated using Debye- Scherrer equation from the width of the XRD peaks. The XPS, X-ray photoelectron spectroscopic analysis is used to study the surface composition and the oxidation state of the synthesized samples. The XPS spectrum was recorded using K-ALPHA (Thermo Fisher Scientific, USA) equipped with a monochromatic X-ray Al K-alpha radiation (10 to 1350 eV), 400 μm spot size at pressure 10^{-9} mbar with full-spectrum pass energy 200 eV and at narrow-spectrum 50 eV.

2.5. Anticancer Activity Studies

2.5.1. Cell Culture

A human Caucasian breast cancer cell line (MCF7) was obtained from the American Type Culture Collection (Rockville, MD, USA). The cancer cells were cultured in DMEM (Dulbecco's Modified Eagle Medium) containing 10% fetal bovine serum (FBS) 100 U/mL of penicillin and streptomycin. The cells were cultivated at 37 °C in a humidified environment with 5% CO_2.

2.5.2. In-Vitro Cytotoxic Activity β-Ni(OH)$_2$ by MTT Assay

MTT, 3-[4,5-dimethyl-2-thiazolyl)-2,5-diphenyl-2H-tetrazolium bromide assay was applied to assess the cytotoxicity of the bio-synthesized β-Ni(OH)$_2$ against the MCF7 cell line. The MTT assay relay on the cleavage of tetrazolium salt by mitochondrial dehydrogenases in live cells [35,36]. Before the MTT assay, the cells were put in 96-well sterilized microplates (5×10^4 cells/well) and kept at 37 °C with DMSO solutions of the test compounds for 48 h in a serum-free medium. The medium culture without the tested compounds was used as a negative control. After incubation, the media in each well was securely removed and replaced with 40 μL of 2.5 mg/mL MTT. Then the samples were incubated for additional 4 h. 200 μL of DMSO was added to solubilize the purple formazan dye crystals. After that, a SpectraMax Paradigm Multi-Mode microplate reader is used to measure the absorbance at 570 nm. The relative cell mortality is the quantification of the mean percentage of dead

cells compared to the control sample [37]. All trials were carried out on different days in triplicate. The obtained values are recorded as the mean ± SD. The probit analysis was performed using SPSS software (SPSS Inc., Chicago, IL, USA) to determine IC_{50} values.

3. Results and Discussions

3.1. Characterization

3.1.1. UV-Vis Spectroscopy

The optical properties of $Ni(OH)_2$-nanocluster and chia seeds extract were evaluated using UV-Vis Spectroscopy. Figure 1a represents the absorption spectra of $Ni(OH)_2$ nanocluster and chia seeds extract. The absorption spectrum of chia seeds extract reveals two main peaks in the range of 250–350 nm. The peak centered at 280 nm could be assigned to the xylose and glucose content of chia extract [38] while the peak at 320 could be attributed to the protein content of the chia seeds extract [39]. Due to its weak light-harvesting characteristics, $Ni(OH)_2$ has more linear absorption spectra in both the UV and visible regions [40].

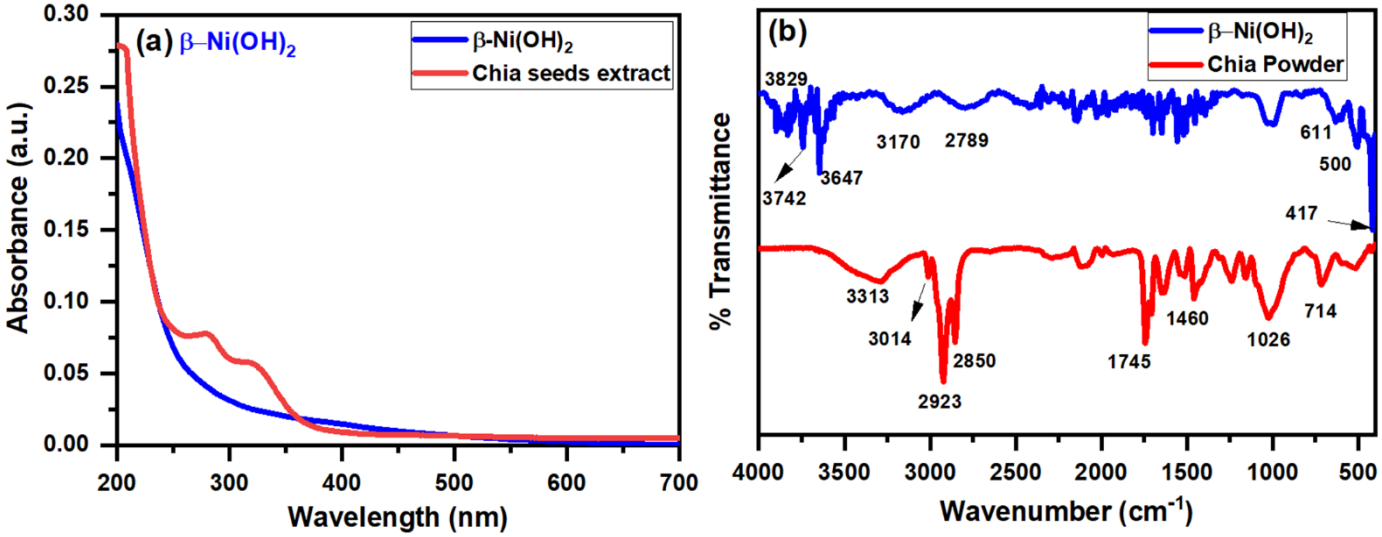

Figure 1. (**a**) UV-Vis spectra and (**b**) FT-IR spectra for chia powder and the biosynthesized β-$Ni(OH)_2$.

3.1.2. FT-IR Spectroscopy

Chia seeds are high in omega-3, polyunsaturated fatty acids, fibers, and proteins, which provide all of the necessary amino acids [41]. FT-IR spectroscopy is performed for chia seeds powder and the synthesized $Ni(OH)_2$ nanocluster to identify the functional groups that are responsible for the reduction and stabilization of the prepared nanocluster. Figure 1b shows the FTIR spectra of chia seeds powder and the bio-synthesized $Ni(OH)_2$ nanoclusters. The chia protein characteristic bands are observed in the region at 3200–3500 cm^{-1}. The broadband at 3300 cm^{-1} is related to the N-H and/or O-H stretching vibration of protein content. The protein amide I groups have characteristic bands in the range 1745–1460 cm^{-1} of C=O bonds. The bands at 2923–2850 cm^{-1} represent the C-H stretching frequency of the methyl and methylene backbones of lipids. The bands at 3014 and 1645 cm^{-1} represent the C=C of linolenic acid and cis-olefins, respectively. The observed band at 714 cm^{-1} is attributed to the bending vibrations of methylene groups in cis-disubstituted olefins [40,41].

The FT-IR spectrum of β-$Ni(OH)_2$ shows a characteristic stretching vibrational mod at 3647 cm^{-1} that represents the nonhydrogen bonded (–O–H) groups present in $Ni(OH)_2$. Whereas the broad peak at 3170 cm^{-1} is assigned to the stretching vibrations of hydrogen-bonded (–O–H) groups [14]. The bands at 611 and 500 cm^{-1} are related to Ni–O–H bending vibrations. The band at 417 cm^{-1} is related to the stretching vibration of the Ni–O

bond [42–44]. The residual function groups of chia seed extract are responsible for the appearance of the bands in the range 1702–1451 cm^{-1} [45]. The results confirm the effective biogenic production of β-$Ni(OH)_2$ nanocluster.

3.1.3. FE-SEM and EDS Analysis

FE-SEM, field emission-scanning electron microscopy, and energy-dispersive X-ray spectroscopy (EDS) are used to investigate the morphological, structure properties, and the composition of the bio-synthesized β-$Ni(OH)_2$ nanocluster. Figure 2a,b show the images of β-$Ni(OH)_2$ with different magnification scales. It can be seen that the synthesized materials seem similar to a cluster of nanoparticles. The chia extract is worked as a capping agent for the particles, and they are probably attached by the hydroxyl groups in the molecules, so it gives the appearance of a nanocluster molecule [45–47].

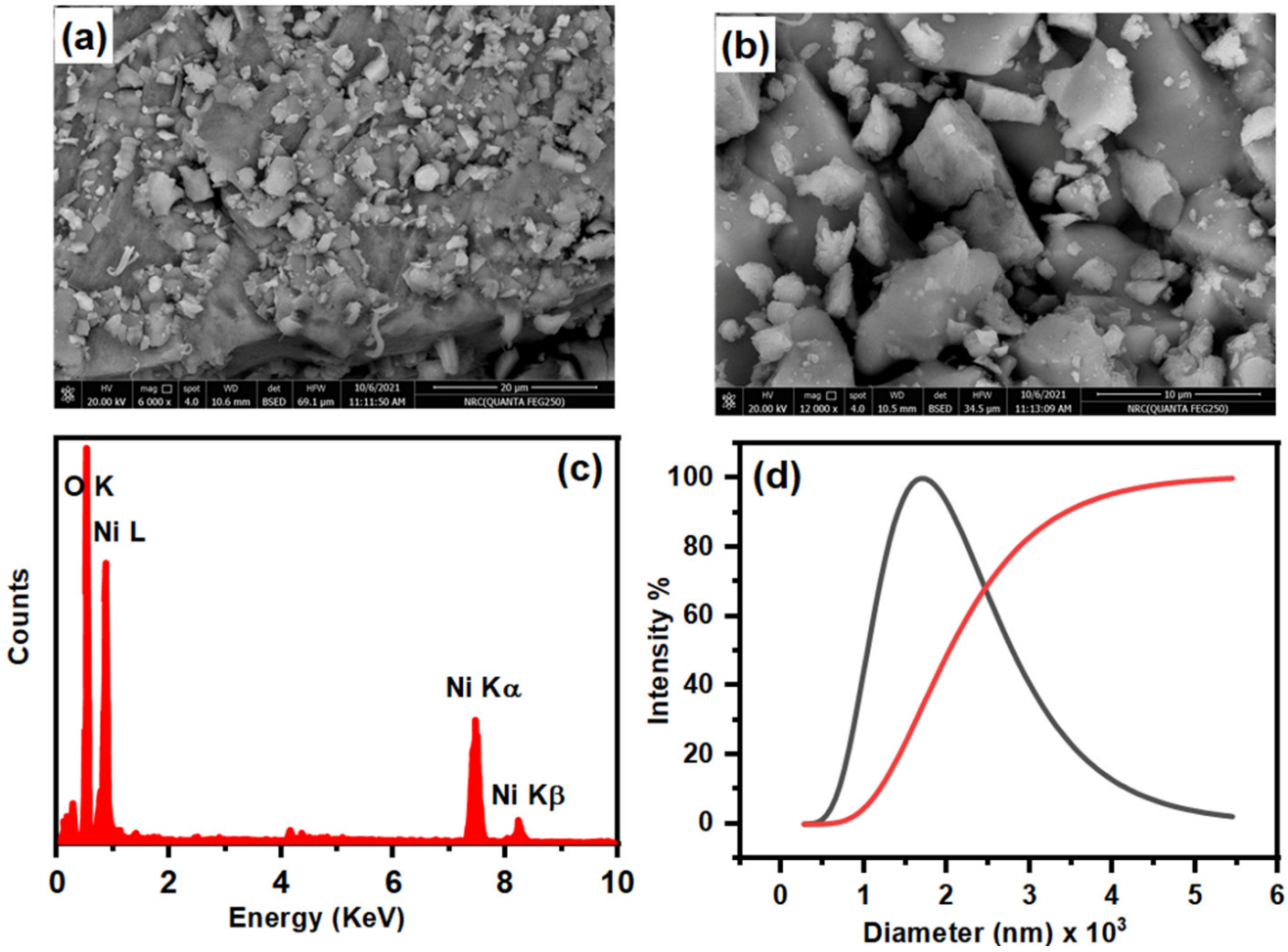

Figure 2. (**a**,**b**) FE-SEM images (**c**) Energy Dispersive Spectroscopy (EDS) and (**d**) Particles size distribution measured by DLS for $Ni(OH)_2$-NC.

Figure 2c shows the energy-dispersive spectroscopy (EDS) microanalysis profile of the β-$Ni(OH)_2$ nanocluster. The data illustrates the existence of Ni and O elements only in the nanoparticles which indicates the purity of the synthesized material [48,49].

3.1.4. HR-TEM and DLS Analysis

Figure 3a,b display HR-TEM images of $Ni(OH)_2$ nanocluster. The HR-TEM images show that $Ni(OH)_2$ exists as hexagonal thin segments. Figure 3d represents the histogram of particle size distribution calculated using ImageJ software. The estimated average particle size of the nanoparticle from the TEM measurement was 5.8 nm with a standard deviation

of 1.48 nm. Figure 2d represents the size distribution for the as-grown nanocluster by the dynamic light scattering (DLS) analysis. The average particle size calculated from DLS is (~2860 nm) with a standard deviation of (~1500 nm). The particle size calculated based on DLS analysis is much greater than that calculated from TEM analysis. TEM measurements reflect only the metal core while the DLS analysis includes the metal core, surface surrounding molecules, and the hydration sphere around the nanoparticle [50]. Another possible explanation for the difference between DLS and TEM particle size measurements is due to the presence of attached layers of different organic molecules (from chia seed extract) to the material nanoparticles, these organic molecules are electron transparent and didn't appear in TEM [51]. These observations suggest the effective production of $Ni(OH)_2$ nanoclusters using chia extract as a capping agent. In the formation of the nanocluster the nickel ions associate with the chia extract molecule as a capping agent. Finally, after completing the nucleation stage, coalescence, Ostwald-ripening, and growth steps $Ni(OH)_2$ nanocluster was formed [46]. SAED, the selected area electron diffraction, the pattern of $Ni(OH)_2$ nanocluster is shown in Figure 3c, which reveals multi-layered patterns, indicating the polycrystalline nature of the produced $Ni(OH)_2$ nanocluster [52].

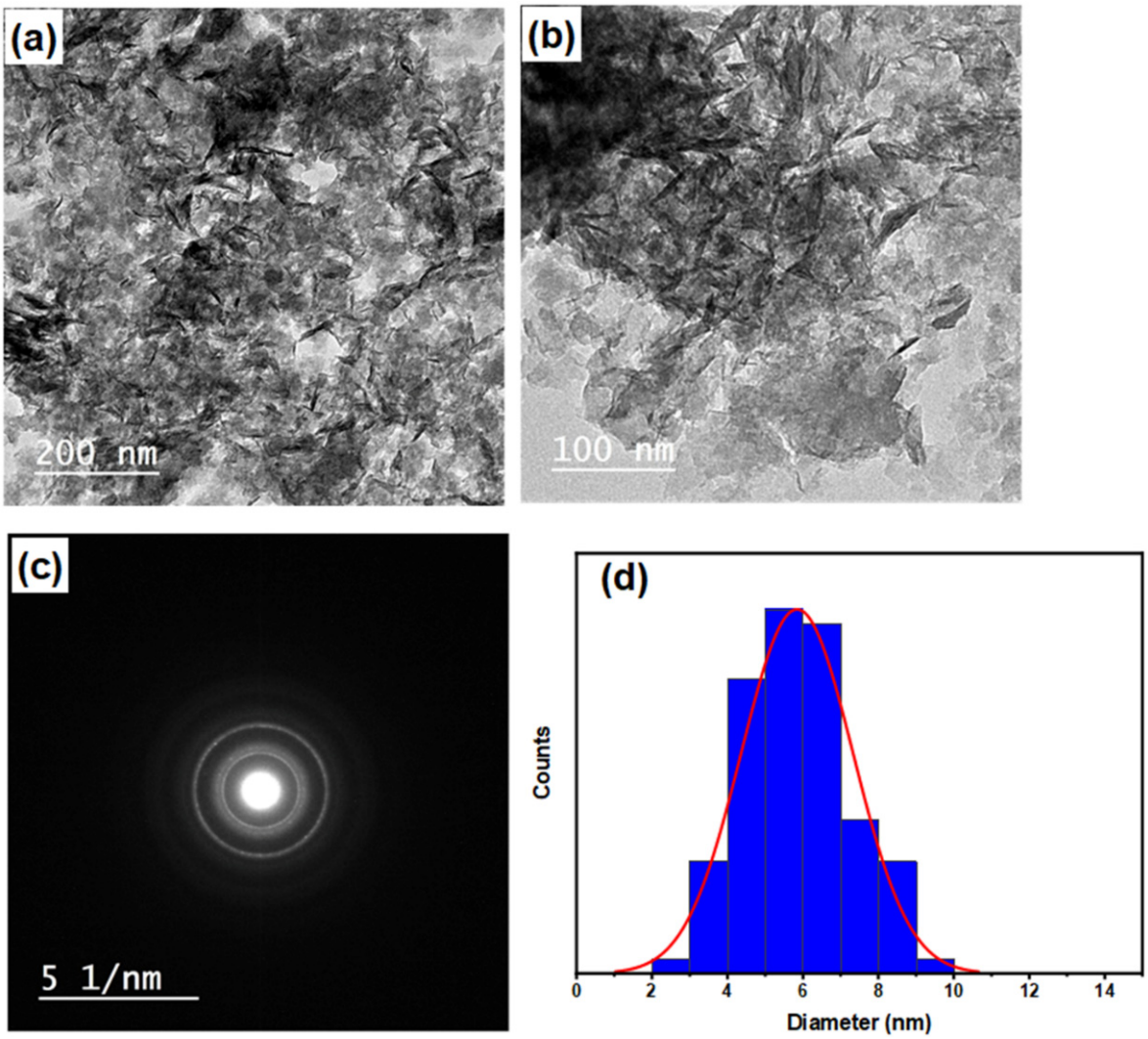

Figure 3. (**a**,**b**) HR-TEM images (**c**) SAED pattern and (**d**) particle size distribution calculated from TEM for β-$Ni(OH)_2$ nanoparticles.

3.1.5. XRD Analysis

The crystal phase of the prepared $Ni(OH)_2$ nanocluster was examined by X-ray diffraction spectroscopy. Figure 4 shows the XRD pattern of the $Ni(OH)_2$ nanocluster. The peaks at 2θ values of 19.2°, 33.1°, 38.5°, 39.0°, 52.1°, and 59.5° can be assigned to the diffraction plans (001), (100), (101), (002), (102) and (110), respectively [53,54]. The resulting diffraction pattern matches the reference pattern of the Theophrasite form of β-$Ni(OH)_2$ with a hexagonal crystal system according to pdf card number # 014-0117 [55]. The crystallite size of the particles can be estimated by applying the Scherrer Equation (1) [56]:

$$D = \frac{K\lambda}{\beta cos\theta} \quad (1)$$

where D is the average particle diameter, K = 0.9 and is related to the crystallite shape, λ refers to the X-ray radiation wavelength and equals 0.15406 Å, θ is the peak angle, and β is the width at half maximum (FHWM) of the corresponding XRD peak. The average particle size is determined using the Scherrer equation for β-$Ni(OH)_2$ nanocluster and found to be 5.5 nm which agrees with the estimated average size from TEM analysis.

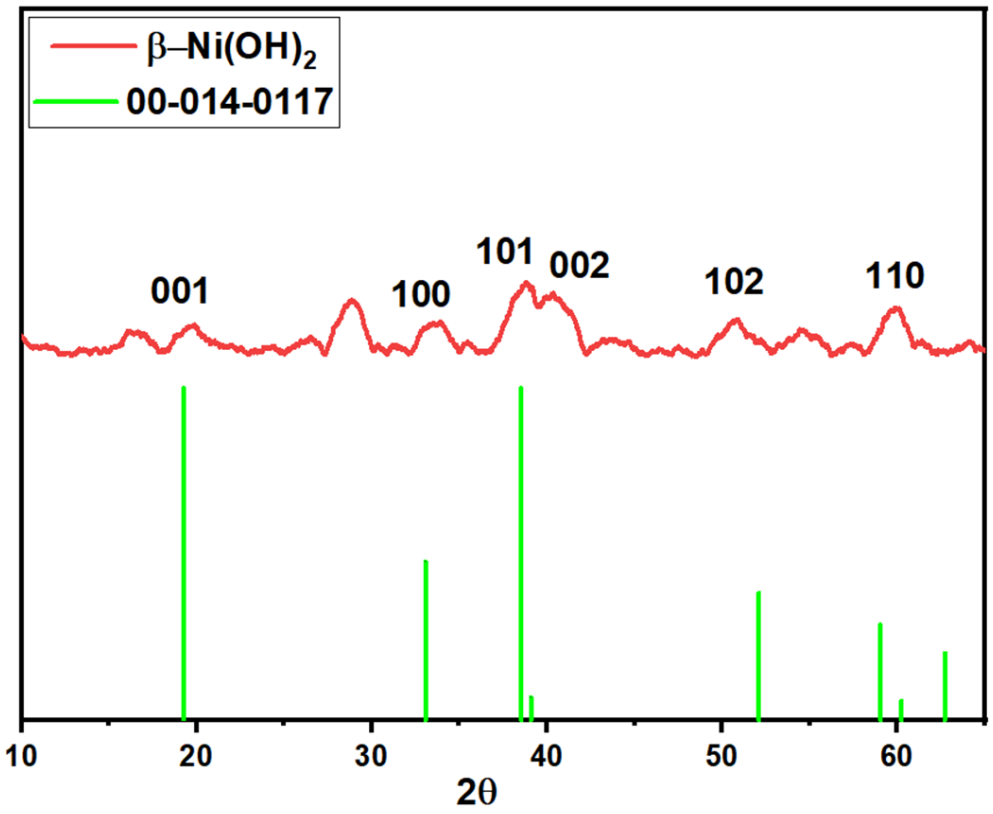

Figure 4. X-Ray Diffraction of Synthesized β-$Ni(OH)_2$ nanocluster.

3.1.6. X-ray Photoelectron Spectroscopy (XPS) Analysis

The XPS analysis was performed to study the elemental compositions of the Ni nanoparticle's surface. Figure 5a shows the survey scan spectrum which indicates the presence of Ni, O, and C elements in the synthesized sample. Figure 5b represents the Ni 2p high-resolution spectrum that contains two spin-orbit doublets of Ni $2p_{3/2}$ and Ni $2p_{1/2}$ components at binding energies of 856.6 and 874 eV, respectively with a spin energy separation of 17.4 eV as previously reported for Ni^{2+} in β-$Ni(OH)_2$ [53]. Furthermore, the peaks at 862.5 and 879.8 eV are attributed to the shake-up structures of Ni 2p. The de-convolution of the Ni $2p_{3/2}$ peak results in two peaks located at 856.6 and 860.2 eV, in

agreement with the BE values reported for Ni^{2+} and Ni^{3+}. The presence of Ni^{3+} on the surface of NP may be due to surface oxidation of β-$Ni(OH)_2$ by air [57].

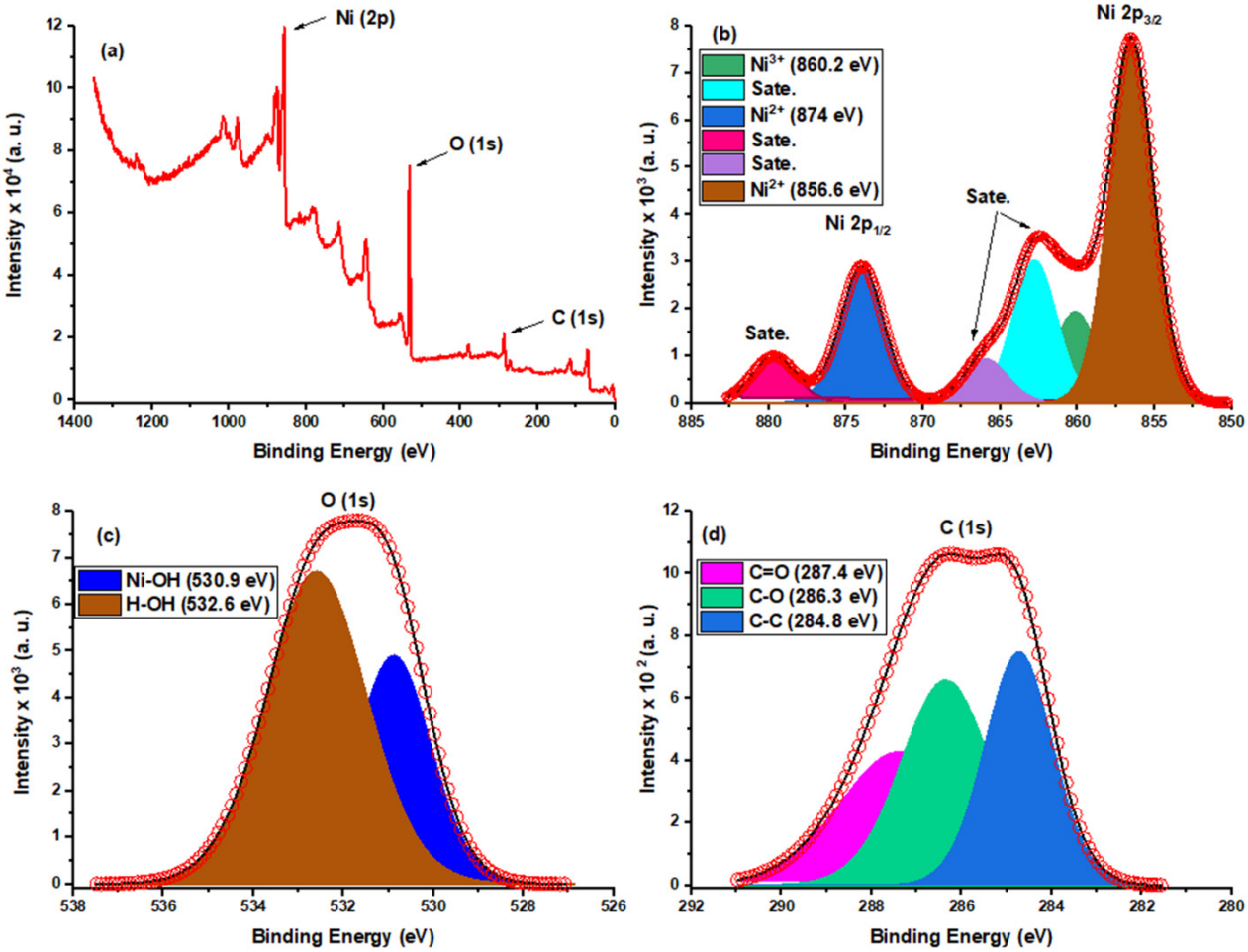

Figure 5. X-ray photoelectron (**a**) Survey scan (**b**) Ni (2p) (**c**) O (1s) and (**d**) C (1s) spectra for the synthesized β-$Ni(OH)_2$ nanocluster.

The XPS spectrum of O 1s is shown in Figure 5c. It has a broad peak that The peak at 531.7 eV that can be de-convoluted into two components: the one at 530.9 eV relates to the characteristic oxygen band in (Ni–OH), whereas the peak at 532.6 eV refers to the (–O–H) group of absorbed water molecules (H–OH) on Ni–NP surface, which appears to agree with the previous results of β-$Ni(OH)_2$ [58].

The C 1s spectrum of XPS consists of one main peak as shown in Figure 5d. This peak can be de-convoluted to three characteristic peaks at 284.8, 286.3, and 287.4 eV, which are related to C–C, C–O, and C=O, respectively [59]. The presence of C in the β-$Ni(OH)_2$ environment is related to the chia extract used in the biogenic synthesis of the material and is proof of the formation of the nanocluster [43]. The binding energy, FWHM, and the atomic percentages of all peaks are listed in Table 1.

Table 1. Binding energy (eV), FWHM, and atomic percentage for the synthesized β-$Ni(OH)_2$.

β-$Ni(OH)_2$	Peak (BE)	FWHM (eV)	Atomic%
Ni 2p	857.27	5.52	22.95
O 1s	532.77	4.26	58.95
C 1s	286.51	4.35	18.01

3.2. Cytotoxicity Evaluation of β-Ni(OH)$_2$

Due to the fast developments in the field of nanotechnology, an enormous number of nanomaterials with distinctly shaped nanostructures were produced by different methods [60]. The metal hydroxide and oxide nanostructured materials have a variety of applications due to their distinct properties, such as large surface area, strong reactivity, and small size in the form of various-shaped nanostructures, which are extensively employed as commercial goods such as cosmetics products, food products, medications, textiles, and other applications. Due to their small sizes, nanomaterials may readily penetrate living cells and influence different human organs. Scheme 1 displays the possible mechanism of the cytotoxic effect of nanomaterials as previously reported in the literature [13,61]. The produced nanoparticles may trigger cell death by interacting with the cells, altering the balance between the oxidants and reductants, and generating reactive oxygen species (ROS). The produced ROS species increase the cytosolic Ca^{2+} concentration or trigger the translocation of transcription factors to the nucleus subsequently assembling pro-inflammatory genes. On the other hand, increasing oxidative stress may stimulate the antioxidant defense system and even lead to cell death [62].

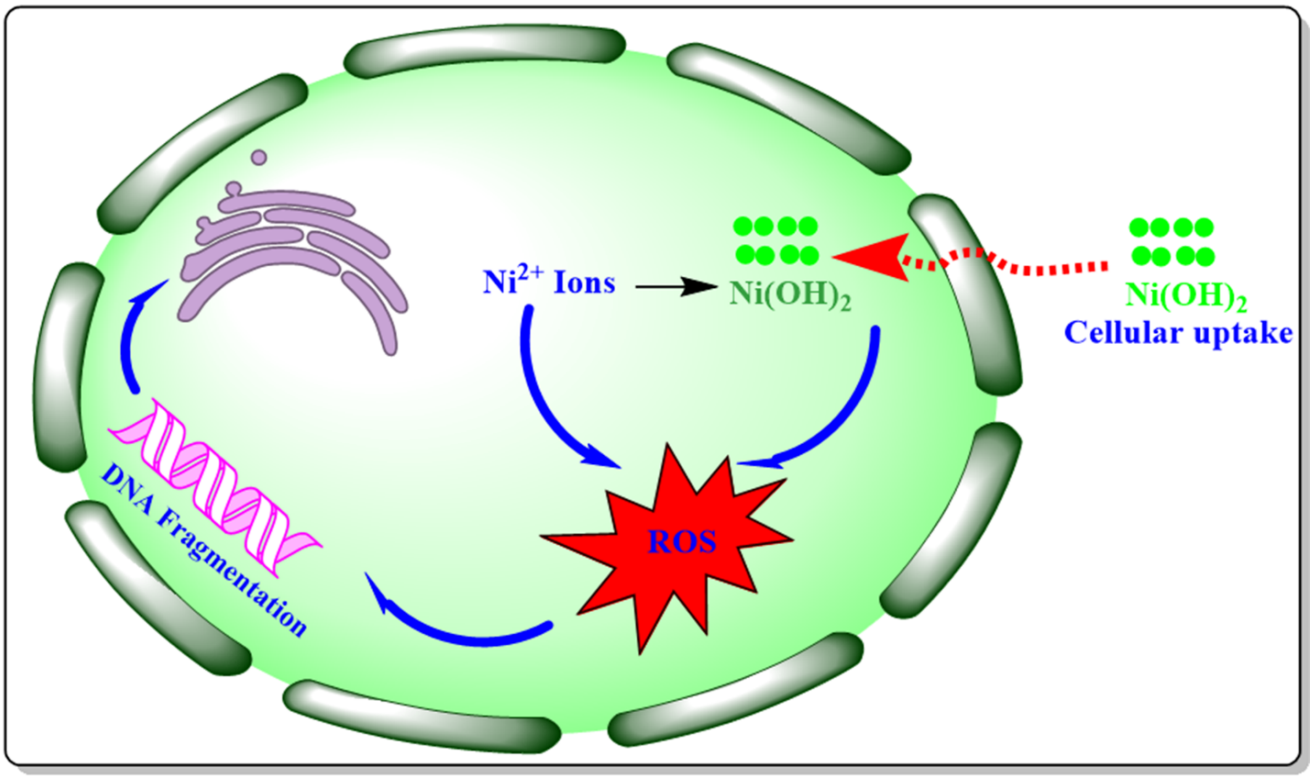

Scheme 1. The possible mechanism of the cytotoxic effect of nanomaterials.

In this work, the human breast cancer cell line MCF7 was used to evaluate the cytotoxicity effect of the bio-synthesized β-Ni(OH)$_2$ using an MTT assay. Figure 6 shows the cell death percentage at different concentrations of β-Ni(OH)$_2$ in the range (1.0–100 μg/mL). The cytotoxic effect of β-Ni(OH)$_2$ is increasing with increasing the concentration of Ni(OH)$_2$ nanocluster indicating a dose-dependent effect on the MCF7 cell line. The IC_{50} value calculated was 62.7 μg/mL and the maximum cell death was found to be 83.2 at 100 ppm.

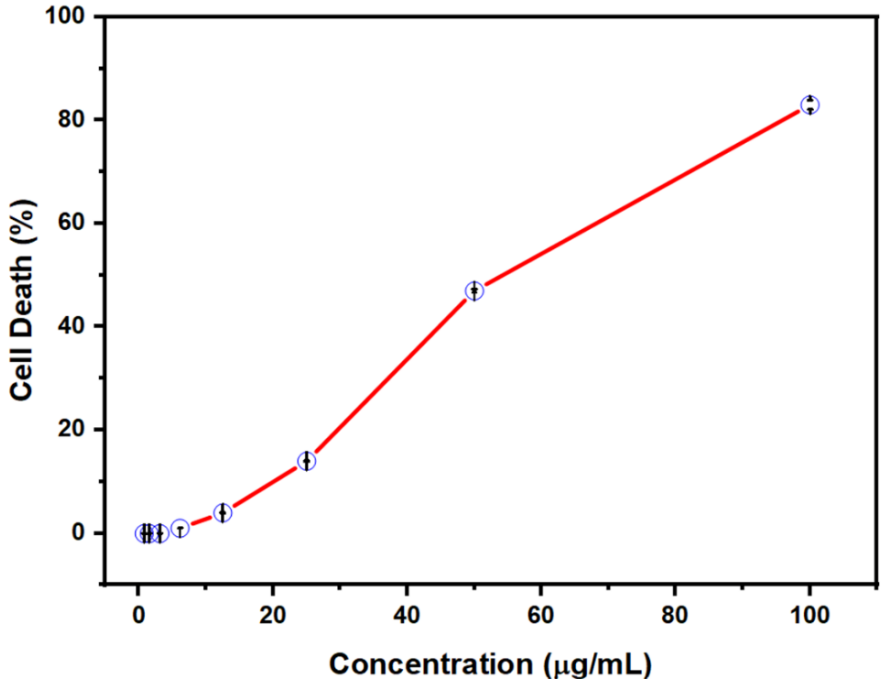

Figure 6. Cell death percentage at different β-Ni(OH)$_2$ concentrations.

4. Conclusions

In this study, β-Ni(OH)$_2$ nanocluster have been synthesized successfully in an aqueous medium by sonication chia seeds extract as a capping and reducing agent. Different analysis techniques were used to study nanoclusters' physical and chemical properties. According to the results, the synthesized materials are on the nanoscale and have a cluster shape with an average particle size of 5.8 nm as measured by TEM. SEM, EDS, and XRD results indicate that the produced nanoparticles reveal a hexagonal shape of the Theopharasite form of pure β-Ni(OH)$_2$. The XPS results show the presence of peaks related to Ni2+, Ni-OH, O-H, C-C, C-O, and C=O confirming the successful biogenic synthesis of Ni(OH)$_2$ nanocluster. The in-vitro cytotoxic activity β-Ni(OH)$_2$ nanocluster synthesized by using chia seeds extract was tested by using MTT assay. The cytotoxicity of β-Ni(OH)$_2$ nanocluster was measured on the MCF7 cell line. The results reveal that β-Ni(OH)$_2$ nanocluster were found to be toxic to the studied cell lines with a maximum cell death percentage of 83.2% at 100 ppm of the samples. The number of dead cells indicated the association of the dose toxicity along with a concentration-dependent exposure time.

Author Contributions: Conceptualization, H.A.H. and A.T.; methodology, H.A.H. and A.T.; validation, H.A.H. and A.T.; formal analysis, H.A.H. and A.T.; investigation, H.A.H. and A.T.; resources, H.A.H. and A.T.; data curation, H.A.H. and A.T.; writing—original draft preparation, H.A.H. and A.T.; writing—review and editing, H.A.H. and A.T.; visualization, H.A.H. and A.T.; supervision, H.A.H. and A.T.; project administration, H.A.H.; funding acquisition, H.A.H. All authors have read and agreed to the published version of the manuscript.

Funding: The authors extend their appreciation to the Deanship of Scientific Research at King Faisal University for funding this research through project number **AN000257**.

Institutional Review Board Statement: The study was conducted in accordance with the Declaration of Helsinki and approved by the Research Ethics Committee at King Faisal University (reference number "KFU-REC-2022-MAR-EA000516", approval date 22 March 2022) for studies involving human Cell lines.

Conflicts of Interest: The authors declare that they have no known competing financial interests or personal relationships that could have appeared to influence the work reported in this paper.

References

1. Cheng, M.Y.; Hwang, B.J. Control of uniform nanostructured α-$Ni(OH)_2$ with self-assembly sodium dodecyl sulfate templates. *J. Colloid Interface Sci.* **2009**, *337*, 265–271. [CrossRef] [PubMed]
2. Saghatforoush, L.A.; Hasanzadeh, M.; Sanati, S.; Mehdizadeh, R. $Ni(OH)_2$ and NiO nanostructures: Synthesis, characterization and electrochemical performance. *Bull. Korean Chem. Soc.* **2012**, *33*, 2613–2618. [CrossRef]
3. Lai, X.; Wei, Y.; Zhao, H.; Chen, S.; Bu, X.; Lu, F.; Qu, D.; Yao, L.; Zheng, J.; Zhang, J. The effect of Fe_2O_3 and ZnO nanoparticles on cytotoxicity and glucose metabolism in lung epithelial cells. *J. Appl. Toxicol.* **2015**, *35*, 651–664. [CrossRef] [PubMed]
4. Borah, D.; Yadav, A.K. A Novel 'Green' Synthesis of Antimicrobial Silver Nanoparticles (AgNPs) by using Garcinia morella (Gaertn) Desr. Fruit Extract. *Nanosci. Nanotechnol.-Asia* **2015**, *5*, 25–31. [CrossRef]
5. Gupta, A.K.; Gupta, M. Cytotoxicity suppression and cellular uptake enhancement of surface modified magnetic nanoparticles. *Biomaterials* **2005**, *26*, 1565–1573. [CrossRef]
6. Wang, Y.; He, X.; Wang, K.; Zhang, X.; Tan, W. Barbated Skullcup herb extract-mediated biosynthesis of gold nanoparticles and its primary application in electrochemistry. *Colloids Surf. B Biointerfaces* **2009**, *73*, 75–79. [CrossRef]
7. Haigh, P.A. *Visible Light*; IOP Publishing: Bristol, UK, 2020. [CrossRef]
8. Lozano, T.; Rey, M.; Rojas, E.; Moya, S.; Fleddermann, J.; Estrela-Lopis, I.; Donath, E.; Wang, B.; Mao, Z.; Gao, C.; et al. Cytotoxicity effects of metal oxide nanoparticles in human tumor cell lines. *J. Phys. Conf. Ser.* **2011**, *304*, 012046. [CrossRef]
9. Cambre, M.H.; Holl, N.J.; Wang, B.; Harper, L.; Lee, H.J.; Chusuei, C.C.; Hou, F.Y.S.; Williams, E.T.; Argo, J.D.; Pandey, R.R.; et al. Cytotoxicity of NiO and $Ni(OH)_2$ nanoparticles is mediated by oxidative stress-induced cell death and suppression of cell proliferation. *Int. J. Mol. Sci.* **2020**, *21*, 2355. [CrossRef]
10. Forest, V.; Leclerc, L.; Hochepied, J.-F.; Trouvé, A.; Sarry, G.; Pourchez, J. Impact of cerium oxide nanoparticles shape on their in vitro cellular toxicity. *Toxicol. Vitr.* **2017**, *38*, 136–141. [CrossRef]
11. Boskabadi, S.H.; Balanezhad, S.Z.; Neamati, A.; Tabrizi, M.H. The green-synthesized zinc oxide nanoparticle as a novel natural apoptosis inducer in human breast (MCF7 and MDA-MB231) and colon (HT-29) cancer cells. *Inorg. Nano-Metal Chem.* **2021**, *51*, 733–743. [CrossRef]
12. Di Bucchianico, S.; Gliga, A.R.; Åkerlund, E.; Skoglund, S.; Wallinder, I.O.; Fadeel, B.; Karlsson, H.L. Calcium-dependent cyto- and genotoxicity of nickel metal and nickel oxide nanoparticles in human lung cells. *Part. Fibre Toxicol.* **2018**, *15*, 32. [CrossRef] [PubMed]
13. Kai, W.; Xiaojun, X.; Ximing, P.; Zhenqing, H.; Qiqing, Z. Cytotoxic effects and the mechanism of three types of magnetic nanoparticles on human hepatoma BEL-7402 cells. *Nanoscale Res. Lett.* **2011**, *6*, 480. [CrossRef] [PubMed]
14. Tientong, J.; Garcia, S.; Thurber, C.R.; Golden, T.D. Synthesis of nickel and nickel hydroxide nanopowders by simplified chemical reduction. *J. Nanotechnol.* **2014**, *2014*, 193162. [CrossRef]
15. Kang, G.S.; Gillespie, P.A.; Chen, L.C. Inhalation exposure to nickel hydroxide nanoparticles induces systemic acute phase response in mice. *Toxicol. Res.* **2011**, *27*, 19–23. [CrossRef] [PubMed]
16. Kovalenko, V.; Kotok, V. Synthesis OF $Ni(OH)_2$, Suitable For Supercapacitor Application, By The Cold Template Homogeneous Precipitation Method. *East.-Eur. J. Enterp. Technol.* **2021**, *2*, 45–51. [CrossRef]
17. Vinichenko, Y.P.; Sidorova, E.N. Synthesis and characterization of nickel hydroxide nanoparticles obtained by chemical deposition method under different precipitation conditions. *J. Phys. Conf. Ser.* **2016**, *741*, 12194. [CrossRef]
18. Krishnakumar, B.; Alsalme, A.; Alharthi, F.A.; Mani, D.; Anandan, K.; Amutha, P.; Sobral, A.J.F.N. Synthesis, characterization of gelatin assisted ZnO and its effective utilization of toxic azo dye degradation under direct sunlight. *Opt. Mater.* **2021**, *113*, 110854. [CrossRef]
19. Hua, J. Synthesis and characterization of gold nanoparticles (AuNPs) and ZnO decorated zirconia as a potential adsorbent for enhanced arsenic removal from aqueous solution. *J. Mol. Struct.* **2021**, *1228*, 129482. [CrossRef]
20. Nasrollahzadeh, M.; Mohammad Sajadi, S. Green synthesis of copper nanoparticles using Ginkgo biloba L. leaf extract and their catalytic activity for the Huisgen [3+2] cycloaddition of azides and alkynes at room temperature. *J. Colloid Interface Sci.* **2015**, *457*, 141–147. [CrossRef]
21. Salmani, M.H.; Abedi, M.; Mozaffari, S.A.; Mahvi, A.H.; Sheibani, A.; Jalili, M. Simultaneous reduction and adsorption of arsenite anions by green synthesis of iron nanoparticles using pomegranate peel extract. *J. Environ. Health Sci. Eng.* **2021**, *19*, 603–612. [CrossRef]
22. Nundy, S.; Eom, T.Y.; Song, K.Y.; Park, J.S.; Lee, H.J. Hydrothermal synthesis of mesoporous ZnO microspheres as NOX gas sensor materials—Calcination effects on microstructure and sensing performance. *Ceram. Int.* **2020**, *46*, 19354–19364. [CrossRef]
23. Baykal, A.; Kavas, H.; Durmuş, Z.; Demir, M.; Kazan, S.; Topkaya, R.; Toprak, M.S. Sonochemical synthesis and chracterization of Mn_3O_4 nanoparticles. *Cent. Eur. J. Chem.* **2010**, *8*, 633–638. [CrossRef]
24. Muthukrishnaraj, A.; Kalaivani, S.S.; Manikandan, A.; Kavitha, H.P.; Srinivasan, R.; Balasubramanian, N. Sonochemical synthesis and visible light induced photocatalytic property of reduced graphene oxide@ZnO hexagonal hollow rod nanocomposite. *J. Alloys Compd.* **2020**, *836*, 155377. [CrossRef]
25. Da'na, E.; Taha, A.; Afkar, E. Green synthesis of iron nanoparticles by Acacia nilotica pods extract and its catalytic, adsorption, and antibacterial activities. *Appl. Sci.* **2018**, *8*, 1922. [CrossRef]
26. Usman Ahme, M.; Noseh Dahi, J.; Yada Sudi, I.; Gabriel, S.; Kulini Joh, I. Green Synthesis of Manganese Oxide Nanoparticles from Cassia tora Leaves and its Toxicological Evaluation. *Asian J. Appl. Sci.* **2020**, *13*, 60–67. [CrossRef]

27. Kasthuri, J.; Veerapandian, S.; Rajendiran, N. Biological synthesis of silver and gold nanoparticles using apiin as reducing agent. *Colloids Surf. B Biointerfaces* **2009**, *68*, 55–60. [CrossRef] [PubMed]
28. Roy, P.; Das, B.; Mohanty, A.; Mohapatra, S. Green synthesis of silver nanoparticles using Azadirachta indica leaf extract and its antimicrobial study. *Appl. Nanosci.* **2017**, *7*, 843–850. [CrossRef]
29. Hrnčič, M.K.; Ivanovski, M.; Cör, D.; Knez, Ž. Chia Seeds (*Salvia hispanica* L.): An overview-phytochemical profile, isolation methods, and application. *Molecules* **2020**, *25*, 11. [CrossRef]
30. Nasrollahzadeh, M.; Sajadi, S.M. Synthesis and characterization of titanium dioxide nanoparticles using Euphorbia heteradena Jaub root extract and evaluation of their stability. *Ceram. Int.* **2015**, *41*, 14435–14439. [CrossRef]
31. Joshi, N.; Pathak, A.; Anupam, R.; Jain, N.; Singh, J.; Upadhyaya, C.P. A Rapid and Efficient Biosynthesis of Metallic Nanoparticles Using Aqueous Extract of Chia (*Salvia hispanica* L.) Seeds. *Bionanoscience* **2019**, *9*, 893–902. [CrossRef]
32. de Falco, B.; Amato, M.; Lanzotti, V. Chia seeds products: An overview. *Phytochem. Rev.* **2017**, *16*, 745–760. [CrossRef]
33. Divyapriya, G.K.; Veeresh, D.J.; Yavagal, P.C. Evaluation of Antibacterial Efficacy of Chia (*Salvia hispanica*) Seeds Extract Against Porphyromonas Gingivalis, Fusobacterium Nucleatum and Aggregatibacter Actinomycetemcomitans-an in-Vitro Study. *Int. J. Ayurveda Pharma Res.* **2016**, *4*, 2322–2902.
34. Hernández-Morales, L.; Espinoza-Gómez, H.; Flores-López, L.Z.; Sotelo-Barrera, E.L.; Núñez-Rivera, A.; Cadena-Nava, R.D.; Alonso-Núñez, G.; Espinoza, K.A. Study of the green synthesis of silver nanoparticles using a natural extract of dark or white *Salvia hispanica* L. seeds and their antibacterial application. *Appl. Surf. Sci.* **2019**, *489*, 952–961. [CrossRef]
35. Al-Qasmi, N. Facial eco-friendly synthesis of copper oxide nanoparticles using chia seeds extract and evaluation of its electrochemical activity. *Processes* **2021**, *9*, 2027. [CrossRef]
36. El-Sayed, W.A.; Khalaf, H.S.; Mohamed, S.F.; Hussien, H.A.; Kutkat, O.M.; Amr, A.E. Synthesis and antiviral activity of 1,2,3-triazole glycosides based substituted pyridine via click cycloaddition. *Russ. J. Gen. Chem.* **2017**, *87*, 2444–2453. [CrossRef]
37. Hassan, A.S.; Mady, M.F.; Awad, H.M.; Hafez, T.S. Synthesis and antitumor activity of some new pyrazolo[1,5-a]pyrimidines. *Chin. Chem. Lett.* **2017**, *28*, 388–393. [CrossRef]
38. Samrot, A.V.; Lavanya Agnes Angalene, J.; Roshini, S.M.; Stefi, S.M.; Preethi, R.; Raji, P.; Madan Kumar, A.; Suresh Kumar, S. Purification, characterization and exploitation of Azadirachta indica gum for the production of drug loaded nanocarrier. *Mater. Res. Express* **2020**, *7*, 055007. [CrossRef]
39. Jia, S.; Yu, H.; Lin, Y.; Dai, Y. Characterization of extracellular polysaccharides from Nostoc flagelliforme cells in liquid suspension culture. *Biotechnol. Bioprocess Eng.* **2007**, *12*, 271–275. [CrossRef]
40. Barakat, M.A.; Anjum, M.; Kumar, R.; Alafif, Z.O.; Oves, M.; Ansari, M.O. Design of ternary $Ni(OH)_2$/graphene oxide/TiO_2 nanocomposite for enhanced photocatalytic degradation of organic, microbial contaminants, and aerobic digestion of dairy wastewater. *J. Clean. Prod.* **2020**, *258*, 120588. [CrossRef]
41. Darwish, A.M.G.; Khalifa, R.E.; El Sohaimy, S.A. Functional Properties of Chia Seed Mucilage Supplemented In Low Fat Yoghurt. *Alex. Sci. Exch. J.* **2018**, *39*, 450–459. [CrossRef]
42. Archana, G.; Sabina, K.; Babuskin, S.; Radhakrishnan, K.; Fayidh, M.A.; Azhagu Saravana Babu, P.; Sivarajan, M.; Sukumar, M. Preparation and characterization of mucilage polysaccharide for biomedical applications. *Carbohydr. Polym.* **2013**, *98*, 89–94. [CrossRef] [PubMed]
43. Kumar, R.; Sahoo, S.; Joanni, E.; Singh, R.K.; Tan, W.K.; Kar, K.K.; Matsuda, A. Recent progress in the synthesis of graphene and derived materials for next generation electrodes of high performance lithium ion batteries. *Prog. Energy Combust. Sci.* **2019**, *75*, 100786. [CrossRef]
44. Saleem, S.; Ahmed, B.; Khan, M.S.; Al-Shaeri, M.; Musarrat, J. Inhibition of growth and biofilm formation of clinical bacterial isolates by NiO nanoparticles synthesized from Eucalyptus globulus plants. *Microb. Pathog.* **2017**, *111*, 375–387. [CrossRef]
45. Hassanin, H.A.; Taha, A.; Afkar, E. Novel bio-mediated Ag/Co_3O_4 nanocomposites of different weight ratios using aqueous neem leaf extract: Catalytic and microbial behaviour. *Ceram. Int.* **2020**, *47*, 3099–3107. [CrossRef]
46. Vijayakumar, S.; Muralidharan, G. Electrochemical supercapacitor behaviour of α-$Ni(OH)_2$ nanoparticles synthesized via green chemistry route. *J. Electroanal. Chem.* **2014**, *727*, 53–58. [CrossRef]
47. Shamish, Z.; Zohar, M.; Shamir, D.; Burg, A. Controlling the size and pattern pitch of $ni(OH)_2$ nanoclusters using dip-pen nanolithography to improve water oxidation. *Molecules* **2020**, *25*, 2937. [CrossRef]
48. Wang, H.Y.; Li, D.G.; Zhu, H.L.; Qi, Y.X.; Li, H.; Lun, N.; Bai, Y.J. Mn_3O_4/$Ni(OH)_2$ nanocomposite as an applicable electrode material for pseudocapacitors. *Electrochim. Acta* **2017**, *249*, 155–165. [CrossRef]
49. Parsaee, Z. Synthesis of novel amperometric urea-sensor using hybrid synthesized NiO-NPs/GO modified GCE in aqueous solution of cetrimonium bromide. *Ultrason. Sonochem.* **2018**, *44*, 120–128. [CrossRef]
50. MacCuspie, R.I.; Rogers, K.; Patra, M.; Suo, Z.; Allen, A.J.; Martin, M.N.; Hackley, V.A. Challenges for physical characterization of silver nanoparticles under pristine and environmentally relevant conditions. *J. Environ. Monit.* **2011**, *13*, 1212–1226. [CrossRef]
51. Lim, J.; Yeap, S.P.; Che, H.X.; Low, S.C. Characterization of magnetic nanoparticle by dynamic light scattering. *Nanoscale Res. Lett.* **2013**, *8*, 381. [CrossRef]
52. Sharma, J.K.; Srivastava, P.; Ameen, S.; Akhtar, M.S.; Singh, G.; Yadava, S. Azadirachta indica plant-assisted green synthesis of Mn_3O_4 nanoparticles: Excellent thermal catalytic performance and chemical sensing behavior. *J. Colloid Interface Sci.* **2016**, *472*, 220–228. [CrossRef] [PubMed]

53. Anantharaj, S.; Karthik, P.E.; Kundu, S. Petal-like hierarchical array of ultrathin $Ni(OH)_2$ nanosheets decorated with $Ni(OH_{)2}$ nanoburls: A highly efficient OER electrocatalyst. *Catal. Sci. Technol.* **2017**, *7*, 882–893. [CrossRef]
54. Klaus, S.; Cai, Y.; Louie, M.W.; Trotochaud, L.; Bell, A.T. Effects of Fe Electrolyte Impurities on $Ni(OH)_2$/NiOOH Structure and Oxygen Evolution Activity. *J. Phys. Chem. C* **2015**, *119*, 7243–7254. [CrossRef]
55. Stern, L.A.; Hu, X. Enhanced oxygen evolution activity by NiO_x and $Ni(OH)_2$ nanoparticles. *Faraday Discuss.* **2014**, *176*, 363–379. [CrossRef] [PubMed]
56. Ted Kroon, R.E. Nanoscience and the scherrer equation versus the "scherrer-gottingen equation". *S. Afr. J. Sci.* **2013**, *109*, 5–6. [CrossRef]
57. Xiong, D.; Li, W.; Liu, L. Vertically aligned porous Nickel(II) hydroxide nanosheets supported on carbon paper with long-term oxygen evolution performance. *Chem. Asian J.* **2017**, *12*, 543–551. [CrossRef] [PubMed]
58. Li, T.; Li, G.H.; Li, L.H.; Liu, L.; Xu, Y.; Ding, H.Y.; Zhang, T. Large-Scale Self-Assembly of 3D Flower-like Hierarchical Ni/Co-LDHs Microspheres for High-Performance Flexible Asymmetric Supercapacitors. *ACS Appl. Mater. Interfaces* **2016**, *8*, 2562–2572. [CrossRef] [PubMed]
59. Koo, W.T.; Kim, S.J.; Jang, J.S.; Kim, D.H.; Kim, I.D. Catalytic Metal Nanoparticles Embedded in Conductive Metal–Organic Frameworks for Chemiresistors: Highly Active and Conductive Porous Materials. *Adv. Sci.* **2019**, *6*, 1900250. [CrossRef]
60. Ahmad, J.; Wahab, R.; Siddiqui, M.A.; Musarrat, J.; Al-Khedhairy, A.A. Zinc oxide quantum dots: A potential candidate to detain liver cancer cells. *Bioprocess Biosyst. Eng.* **2015**, *38*, 155–163. [CrossRef]
61. Akter, M.; Sikder, M.T.; Rahman, M.M.; Ullah, A.A.; Hossain, K.F.B.; Banik, S.; Hosokawa, T.; Saito, T.; Kurasaki, M. A systematic review on silver nanoparticles-induced cytotoxicity: Physicochemical properties and perspectives. *J. Adv. Res.* **2018**, *9*, 1–16. [CrossRef]
62. Khan, S.A.; Kanwal, S.; Rizwan, K.; Shahid, S. Enhanced antimicrobial, antioxidant, in vivo antitumor and in vitro anticancer effects against breast cancer cell line by green synthesized un-doped SnO_2 and Co-doped SnO_2 nanoparticles from Clerodendrum inerme. *Microb. Pathog.* **2018**, *125*, 366–384. [CrossRef] [PubMed]